Hindawi Publishing Corporation
Mathematical Problems in Engineering
Volume 2014, Article ID 240565, 19 pages
http://dx.doi.org/10.1155/2014/240565

Research Article

Accurate Fault Classifier and Locator for EHV Transmission Lines Based on Artificial Neural Networks

Moez Ben Hessine and Souad Ben Saber

Latice Laboratory at Higher National Engineering School of Tunis, ENSIT, University of Tunis, 05 Avenue Taha Hussein, Montfleury, 1008 Tunis, Tunisia

Correspondence should be addressed to Moez Ben Hessine; benhessinemoez@yahoo.fr

Received 6 March 2014; Revised 31 May 2014; Accepted 31 May 2014; Published 15 July 2014

Academic Editor: Haipeng Peng

The ability to identify the fault type and to locate the fault in extra high voltage transmission lines is very important for the economic operation of modern power systems. Accurate algorithms for fault classification and location based on artificial neural network are suggested in this paper. Two fault classification algorithms are presented; the first one uses the single ANN approach and the second one uses the modular ANN approach. A comparative study of two classifiers is done in order to choose which ANN fault classifier structure leads to the best performance. Design and implementation of modular ANN-based fault locator are presented. Three fault locators are proposed and a comparative study of the three fault locators is carried out in order to determine which fault locator architecture leads to the accurate fault location. Instantaneous current and/or voltage samples were used as inputs to ANNs. For fault classification, only the pre-fault and post-fault samples of three-phase currents were used. For fault location, pre-fault and post-fault samples of three-phase currents and/or voltages were used. The proposed algorithms were evaluated under different fault scenarios. Studied simulation results which are presented confirm the effectiveness of the proposed algorithms.

1. Introduction

The design of the high performance protection techniques remains an important subject for the development within the university community and the industry. Indeed, a transmission line is an important element of the electrical power system. Nevertheless, transmission lines present the highest fault appearance rate considering the environmental conditions which are subjected. Hence, the protective relaying systems are integrated in transmission lines to quickly detect faults occurrence and to isolate the faulted part from the rest of power system as soon as possible. These protective relaying systems serve to ensure the power system stability, minimize damage equipment, and restore the service quality. For transmission line protections, various algorithms were proposed in the literature. In the 70s, travelling wave techniques were introduced into the transmission line protection algorithms [1]. However, most researchers [2–4] mentioned that the method founded on the travelling wave does not function well for the faults near the relaying site and for faults having small fault inception angles. The synchronized measurement technology seems to be a promising perspective to obtain real time protection. With the global positioning system (GPS), digital measurement of the three-phase current and voltage signals for the two line ends can be carried out into a synchronous manner [5–8]. These techniques are more precise than the distance relaying protection algorithms which are affected by the insufficient transmission line modeling and the parameter uncertainty due to the aging of lines. Moreover, these techniques require the installation of a GPS where the measurements are synchronized compared to a GPS clock. Nevertheless, the synchronized measurement technology presents many drawbacks as the high cost and the presence of a communication channel between the line terminals which is not available in the majority of lines. Therefore, the fault diagnosis techniques using one-terminal data could be more attractive for researchers. In this context, it is necessary to develop algorithms having the ability to adapt dynamically with the system operating conditions such as the system configuration changes and the fault conditions (fault resistance, fault inception angle, and fault position). Recently, modern technologies of the protection relays are

based on artificial intelligence tools such as fuzzy logic (FL), artificial neural networks (ANNs), and the adaptive network-based fuzzy inference system (ANFIS). Fuzzy logic-based transmission line relaying techniques for fault classification and fault location are proposed by many researchers [9–11]. However, these techniques cannot in any way guarantee precision results**:** for wide variation of faultconditions (high fault resistance, high fault inception angle, and far distance location from relay site). A recent study [12] has proposed an algorithm having the synergy to calculate with high precision the fault locations at distances less than 80% of the line length. In [13] a fault classification algorithm based on fuzzy logic system is presented. Nevertheless, this algorithm is valid only for a less range variety of fault resistance.

Other protection relaying researchers have used the adaptive network-based fuzzy inference system (ANFIS) [14–17]. In [18], a fault detection and classification scheme is developed. This technique uses three-phase currents and zero sequence current but the fault location procedure is not indicated. In [19] a fault classification and location algorithms for combined overhead transmission line have been proposed. The current and voltage samples are used for the proposed scheme. These values were obtained within one cycle after the fault inception that implies a response time superior than one operating cycle. The protection fault approaches based on fuzzy logic (FL) and adaptive network fuzzy inference system (ANFIS) techniques are sensitive to the system frequency variations and require large training sets.

The artificial neural networks were integrated in the protection relaying techniques. These techniques used samples of current and/or voltage without calculating the symmetrical components [1]. Various neural network types such as the multilayer perceptron (MLP), radial basis function (RBF), and probabilistic neural network are applied for fault diagnosis in transmission lines [20–24]. The protection approaches based on ANNs were used for the development of reliable, accurate, and rapid algorithms in real time for fault detection, classification, and location. In this context, [25] developed an application of radial basic function (RBF) neural network applied to fault location in transmission lines. The maximum error of the proposed algorithm is equal to 0.5. Besides, [26, 27] developed neural network approaches for fault detection and fault location in transmission lines. Nevertheless, these approaches detect only the faults which appeared in the first zone of the line, namely, 80% of the transmission line length. In [28] a fault location algorithm for transmission lines was developed. The algorithm uses a single artificial neural network based on the Levenberg-Marquardt optimization technique. However, the fault type is not indicated and the percentage error of the algorithm is maintained below 0.65%. In [29] fault classification and location schemes are proposed. These schemes use three-phase currents and voltages waveforms at one terminal line. The response time of the proposed scheme is not indicated and the percentage error for fault location is equal to 3%. In [30] a new scheme for fault classification and fault location is presented. The maximum error of the proposed scheme is 3.05%, and the response time is not indicated. Reference [31] proposed a fault location module for fault diagnosis which incorporates two stages adaptive structures neural network. The fault detection, classification, and location algorithms are presented with average fault location error of 0.4% and 0.5411%. The results show clearly that this approach leads to a reliable location for all types of faults. The operating time of this method is equal to 1.28 cycles after inception fault. In [32], fault distance and direction estimation based on ANN for protection of doubly fed transmission lines are proposed, but the fault type is not indicated. The operating time of this approach is about 1.5 cycles and the percentage error rate of fault location lies between 0.052% and 1.57%.

In order to develop fault classification and location algorithms leading to desired results with a good precision and fast response time compared to former work, we have proposed in the present paper a new fault classification and location algorithms based on ANNs. Thus, optimal neural networks architecture used in the fault classification and location algorithms (number of hidden layers, number of neurons in hidden layers, reduced training sets, fast convergence to the desired results, and reliability and precision of protection algorithms) were proposed. These algorithms are based on artificial neural networks (ANNs) (feed-forward) trained by a supervised learning algorithm called back-propagation. In this context, two fault classifiers are proposed: the first one uses a single ANN approach and the second one uses a modular ANN approach. A comparative study of the proposed two fault classifiers is carried out in order to determine which reliable and effective ANN fault classifier leads to the best performance. For fault location, three fault locators based on modular ANN approach are proposed in order to choose an optimal architecture strategy with a high precision and fast convergence to the exact fault location. The fault neural classifiers and locators were trained and tested under different fault conditions (fault types, fault locations, fault resistances, and fault inception angles). The simulation results show clearly the high accuracy of the proposed fault classification and location algorithms.

2. Power System under Study

To evaluate the performance of the proposed neural network-based fault detector and locator, a 400 kV, 100 km transmission line extending between two sources is considered in this study. The power system model simulated using MATLAB software is shown in Figure 1. It contains a synchronous generator (driven by hydraulic turbine) connected to an infinite bus. The transmission line has been represented by distributed parameter of one line model using Power System toolbox of MATLAB software and the frequency dependence of the line parameters is taken into account. The proposed fault classification and location algorithms require only the three-phase voltages and/or currents samples at the sending end of the transmission lines. A large number of fault samples data have been generated using MATLAB considering wide variations on fault conditions such as fault locations, fault resistances, fault inception angle, and fault types. Using these data, fault classification and location have been carried out

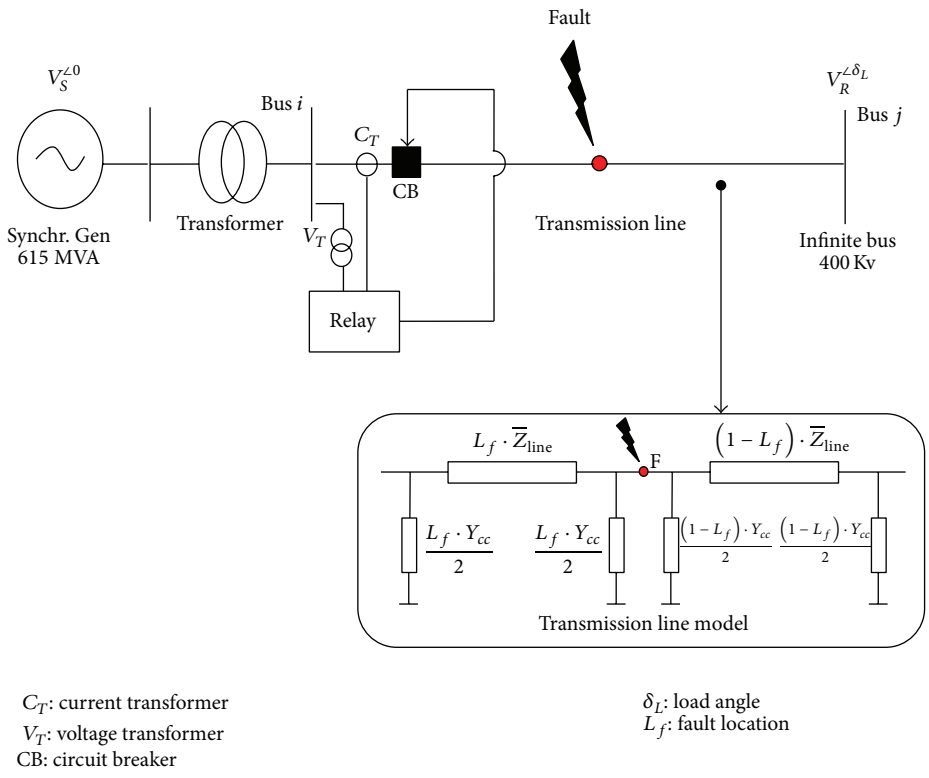

Figure 1: System under study.

by means of MATLAB that make use of its "neural network toolbox."

The transmission line parameters are as follows:

(i) line length = 100 km;

(ii) voltage = 400 Kv;

(iii) transmission line impedance:

(a) positive sequence impedance = 0.0275 + j0.422 Ω/km;

(b) zero sequence impedance = 0.275 + j1.169 Ω/km;

(c) positive sequence capacitance = 9.483 nF/km;

(d) zero sequence capacitance = 6.711 nF/km.

We adopted for the synchronous generator a fourth state order model as follows [33–37]:

$$\begin{aligned}
\frac{dE'_q}{dt} &= \frac{1}{T'_{do}} \cdot \left[E_{fd} - E'_q + \left(X_d - X'_d\right) \cdot I_d\right], \\
\frac{dE'_d}{dt} &= \frac{1}{T'_{qo}} \cdot \left[-E'_d + \left(X_q - X'_q\right) \cdot I_q\right], \\
\frac{d\omega}{dt} &= \frac{1}{M} \cdot \left[P_m - P_e - D \cdot (\omega - 1)\right], \\
\frac{d\delta}{dt} &= \omega - 1,
\end{aligned} \tag{1}$$

where

E'_d , E'_q, and E_{fd} are, respectively, the (d, q) axe transient emf and the emf excitation. X_d, X_q, X'_d, and X'_q are, respectively, the (d, q) axe reactances and the (d, q) axe transient reactances. D is the damping coefficient. M is the inertia constant.

P_e, P_m, ω, and δ are, respectively, the electrical power, mechanical power, speed, and the rotor angle.

In order to identify the fault type and to reach a high degree of accuracy in the location of a fault in transmission lines, a series of contributions have been introduced to estimate the fault distance for transmission lines. Currently, the most widely used method of transmission lines fault location is to determine the apparent reactance of the line during the time that the fault current is flowing and to convert the ohmic result into a distance based on the parameters of the line. It is widely recognized that this method is subject to errors when the fault resistance is high and the line is fed from both ends [38].

There is a need for the measuring algorithms that have the ability to adapt dynamically to the system operating conditions such as changes in the system configuration, source impedances, and fault resistances. Many successful applications based on artificial neural networks to power systems have been demonstrated including security assessment [39] and load forecasting control [40]. Recent applications in protection have covered fault diagnosis for electric power systems [41]. Hence, in order to improve the former work

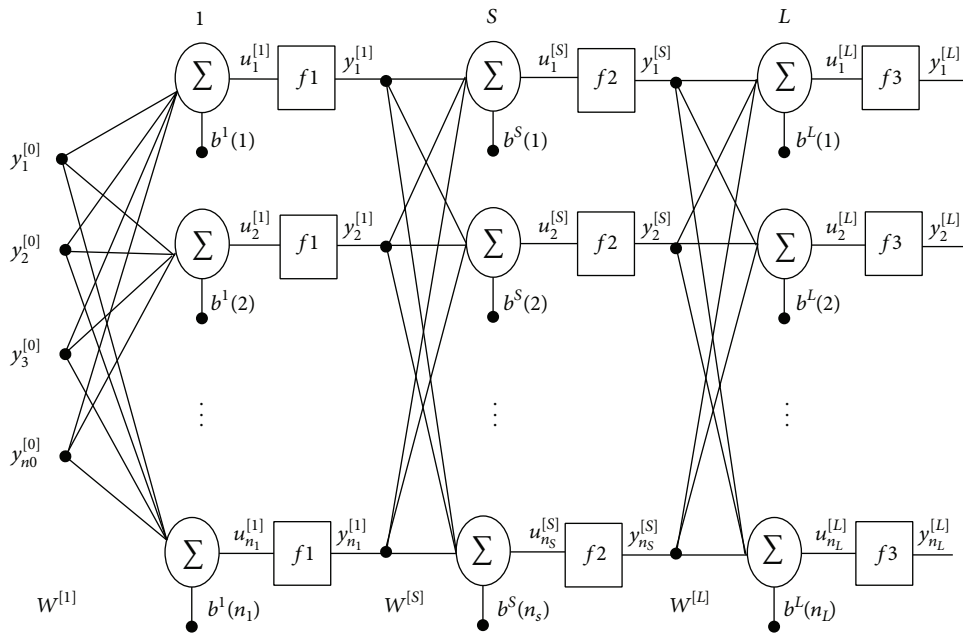

Figure 2: Multilayer network model.

results for fault classification and location in transmission lines, we have resorted towards the artificial neural networks tools.

3. Artificial Neural Networks

The ANN represents a parallel multilayer information processing structure. The characteristic feature of this network is that it considers the accumulated knowledge acquired during training and responds to new events in the most appropriate manner, given the experiences gained during the training process. ANNs imitate the learning process of the human brain and can process problems involving nonlinear and complex data even if the data are imprecise and noisy. The model of the ANN is determined according to network architecture, transfer function, and the learning algorithms. Given their diversification, all the types of neural networks available nowadays cannot be listed easily. The researchers are constantly endeavored to invent new types better suited to resolve specific problems. Among neural networks types, multilayer perceptron (MLP), recurrent neural network, Hopfield neural networks, Kohonen neural networks, and so forth can be cited.

In the recent years, the memristor-based recurrent neural networks represent the main advanced neural network technologies which have been proposed and implemented in various applications fields. Some works of synchronization control problem of this type of networks have been evoked, studied, and discussed by [42].

Authors have employed the differential inclusions theory and the Lyapunov functional method in order to ensure the convergence of the system to the equilibrium point. Furthermore, other several new neural networks architectures have been proposed, namely, the dynamic recurrent neural networks. For these kinds of neural networks, the dynamics analysis study is generally imposed [43–45].

Once the type and the architecture of a neural network are selected for a given application, it is necessary to perform learning algorithms able to determine the weight values allowing the output of the neural network from being as near as possible to the referred aim.

Learning neural network techniques are based on optimization algorithms that seek to minimize the gap between the actual responses of the network and the desired responses, and this by changing the settings successively for any step (called "epochs"). Many learning algorithms have been used such as back-propagation algorithm, conjugate gradient algorithms, quasi-Newton algorithms, and Levenberg-Marquardt algorithm. Recently, new learning algorithm is used for training the ANN such as genetic algorithms GA [46–48], particle swarm optimization algorithm PSO [49–51], and chaotic ant swarm optimization algorithm CAS [52–56].

In this paper, the multilayer perceptron (MLP) neural network was used and trained with a supervised learning algorithm called back-propagation.

3.1. Multilayer Perceptron Neural Network. Multilayer perceptron (MLP) is one of the most frequently used neural network architectures in various applications, and it belongs to the class of supervised neural networks. A typical multilayer (MLP) neural network consists of three layers: an input layer, an output layer, and one or more hidden layers. Each layer consists of a predefined number of neurons. We recall that the neural network is a collection of cells of neurons interconnected by synaptic weights and biases. The inputs are connected to the first hidden layer. Each hidden layer is connected to the next hidden layer, and the last hidden layer is connected to the output layer (Figure 2).

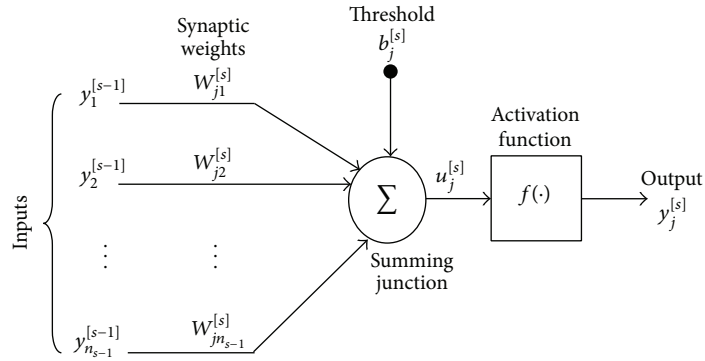

Figure 3: A basic structure of a neuron.

The neuron used is a standard type. It consists in making the sum of all the weighted inputs through its synaptic coefficients which represents the linear output and then applying it to an activation function. The output obtained is then connected to all inputs of the next layer. The basic structure of a neuron is shown in Figure 3.

A neuron mathematical model has a very simple structure compared to a biological neuron [57–59]. Hence, a neuron j can be described mathematically with the following equation:

$$y_j^{[s]} = f\left(b_j^{[s]} + \sum_{i=1}^{n_{s-1}} w_{ji}^{[s]} y_i^{[s-1]}\right), \tag{2}$$

where

f represent the transfer function (activation function) of neuron j;

$\{y_i^{[s-1]}\}$, $i = 1, \ldots, n_{s-1}$, represents the inputs signals of neuron j;

$\{w_{ji}^{[s]}\}$ represents the weight coefficients of the connection between inputs and neuron j;

$b_j^{[s]}$ is the bias of neuron j.

A feed-forward NN consists of input, hidden, and output layers which is considered with P, Q, and R neurons for each layer, respectively. In this structure, $[y^{[P]}] = [y_1^{[P]}, y_2^{[P]}, \ldots, y_P^{[P]}]$ which represents the inputs is applied to the first layer; then, the inputs vectors are transferred to the hidden layer using the connection weight between the input and the hidden layer. The output vector $[y^{[Q]}] = [y_1^{[Q]}, y_2^{[Q]}, \ldots, y_j^{[Q]}, \ldots, y_P^{[Q]}]$ of the hidden layer is then obtained. The neuron output $y_j^{[Q]}$ is determined as follows:

$$y_j^{[Q]} = f_{\text{hidden}}\left(b_j^{[Q]} + \sum_{i=1}^{P} w_{ij}^{[Q]} y_i^{[P]}\right), \tag{3}$$

where

$w_{ij}^{[Q]}$ represents the connection weight between the neuron j in the hidden layer and the ith neuron of the input layer;

$b_j^{[Q]}$ represents the bias of neuron j;

f_{hidden} represents the activation function of the hidden layer.

The values of the vector $y_j^{[Q]}$ of the hidden layer are transferred to the output layer using the connection weight between the hidden layers and the output layer. However, the output vector $[y^{[R]}] = [y_1^{[R]}, y_2^{[R]}, \ldots, y_k^{[R]}, \ldots, y_R^{[R]}]$ of the output layer is determined. The output $y_k^{[R]}$ of the neuron k (on the output layer) is obtained as follows:

$$y_k^{[R]} = f_{\text{out}}\left(b_k^{[R]} + \sum_{j=1}^{Q} w_{jk}^{[R]} y_j^{[Q]}\right). \tag{4}$$

$w_{jk}^{[R]}$ represents the connection weight between the neuron k in the output layer and the jth neuron of the hidden layer.

f_{out} is the activation function of the output layer.

The error in the output layer between the output y_k and its desired value $y_{k\text{-desired}}$ $(y_k - y_{k\text{-desired}})$ is minimized by the mean square error at the output layer, defined as follows:

$$\text{Error} = \frac{1}{2}\sum_{k=1}^{R}\left(y_{k\text{-desired}} - y_k\right)^2. \tag{5}$$

3.2. Back-Propagation Algorithm. Back-propagation training algorithm (BP) is an iterative gradient descent algorithm which is a simple way to train multilayer feed-forward neural networks. The BP algorithm has become the standard algorithm used for training multilayer perceptron. It is a generalized least mean squares (LMS) algorithm that minimizes the sum of the squares of the errors between the actual and the desired outputs. During training, the weights and biases of the network are iteratively adjusted to minimize the network performance function.

The main steps of the back-propagation algorithm are sum raised as in Algorithm 1.

The training data set of an ANN should contain the necessary information to generalize the problem. In this

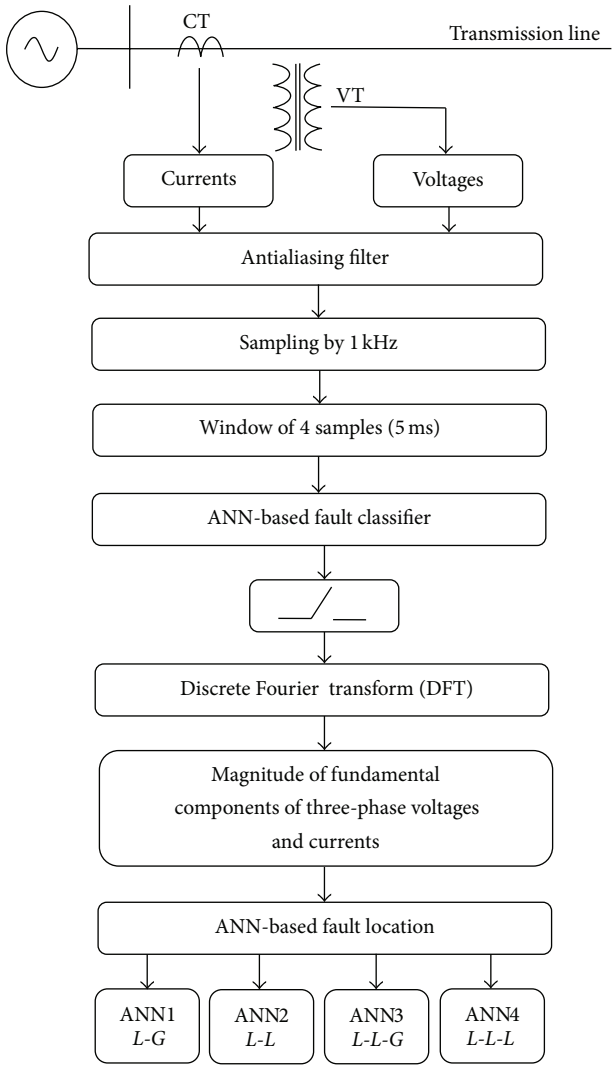

Figure 4: Process for generating inputs patterns to the ANNs fault classifier and fault locator.

work, different combinations of various fault conditions were considered and training patterns were generated by simulating a different fault situation on the power system study. Fault conditions such as fault resistance, fault location, and fault inception angle were changed to obtain training patterns covering a wide range of different power system conditions.

4. Configuration of Fault Classification and Location System Using ANN

The fault classifier and fault locator configuration is shown in Figure 4. The protection relay inputs are presented by the voltage and current waveforms acquired at the line end (relay location) via current transformer CT and voltage transformer VT. These signals are used as inputs to the ANN-based fault classifier and fault locator. The phase current and voltage signals extracted from the simulation at the relay location are processed with an anti-aliasing filter in order to filter the higher order harmonics. A simple 2nd-order low-pass Butter worth filter with cut-off frequency of 400 Hz has been used. Three-phase voltages and currents waveforms are sampled at a sampling frequency of 1 KHz. This sampling rate is compatible with sampling rates presently used in digital relays [38]. Furthermore, a discrete Fourier transform (DFT) is used to extract the fundamental components of these signals which are used as inputs to the ANN-based fault classifier and fault locator. On one side, the proposed fault classifier is designed to identify the fault type and on the other side the fault locator is designed to estimate the exact fault location in the transmission line.

Step. BP.1: Initialization
Initialize random matrices synoptic weight:
$W^{[s]}: s = 1, \ldots, L$
Step.BP.2: Propagation
Calculate for each layer $s = 1, \ldots, L$:
$$u_j^{[s]} = \sum_{i=0}^{n_{s-1}} w_{ji}^{[s]} y_i^{[s-1]}$$
$$y_j^{[s]} = f\left(u_j^{[s]}\right)$$
Step.BP.3: Errors calculation
Calculate local errors for:
(i) Output layer:
$$\delta_{jp}^{[L]} = e_{jp}^{[L]} f'\left(u_{jp}^{[L]}\right)$$
(ii) Layers: $s = L - 1, \ldots, 1$
$$\delta_{jp}^{[s]} = f'\left(u_{jp}^{[s]}\right) \sum_{r=1}^{n_{s+1}} \left(\delta_{jp}^{[s+1]} w_{rj}^{[s+1]}\right)$$
$W^{[s+1]}$ is deprived of its first line
Step.BP.4: Adaptation
Modify the following synaptic weights:
$\Delta w_{ji}^{[s]}(k) = \mu y_{ip}^{[s-1]} \delta_{jp}^{[s]} : s = 1, \ldots, L$
Step.BP.5: Stop test
Test the total squared Error.

Algorithm 1: Steps of the back-propagation algorithm.

The design process of the fault classifier and the fault locator based on ANN is given by the following algorithm depicted in Figure 5.

4.1. Fault Classification

4.1.1. Inputs and Outputs. A feed-forward neural network of three layers trained by the back-propagation algorithm is selected for the fault classification task. In this section, two neural fault classifiers are developed. The first classifier (FC_1) based on the integration of single artificial neural network is used to classify the fault type which can affect a transmission line. The block diagram of the proposed single ANN-based fault classifier (FC_1) is illustrated in Figure 6. The single neural network, conceived for the proposed fault classifier (FC_1), takes into consideration the fundamental signals of the three-phase currents and the zero sequence currents. These signals are sampled at a frequency of 1 kHz (20 samples per 50 Hz cycle). The inputs data for the single ANN-based-fault

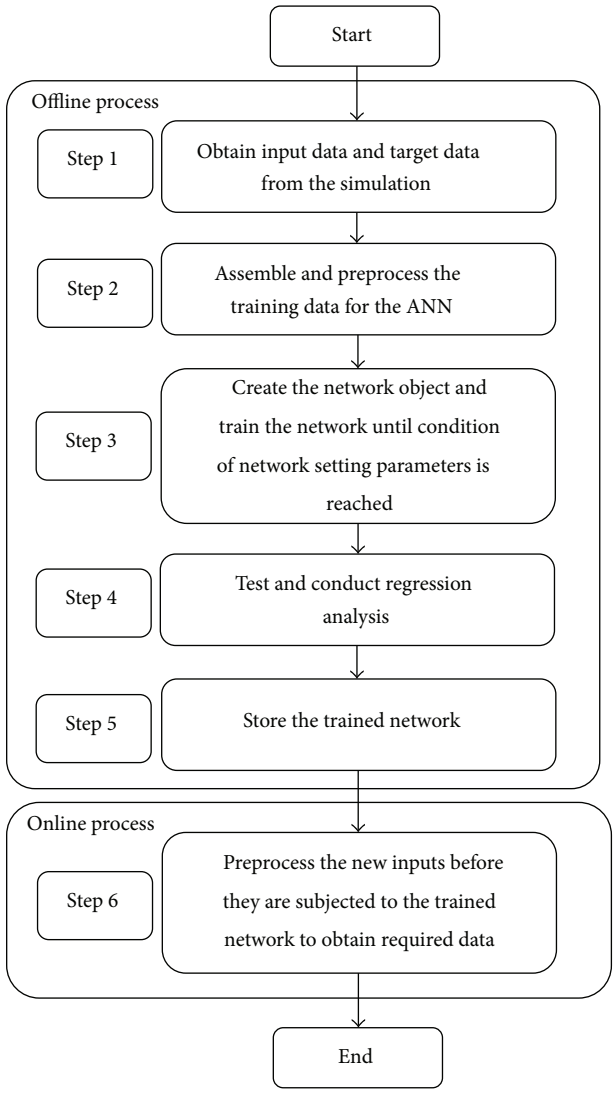

Figure 5: The implementation procedures in the training of the ANN.

classifier are four prefault and four postfault for each phase current and for the zero sequence current.

The $(I_i(k)/I_{i-\mathrm{PF}}(k)$, with $i = \{R, S, T\})$ are the per-unit values calculated by the division of the samples currents in fault time $I_i(k)$ (postfault) to the prefault samples current $I_{i-\mathrm{PF}}(k)$ in related phase. Consequently, the selected input numbers for the fault classification algorithm (FC_1) are equal to 16: four current samples for each phase (R, S and T) and four samples for zero sequence current. The input vector is presented according to the following equation:

$$X_{\mathrm{FC}_1} = \left[\frac{I_R(k)}{I_{R-\mathrm{PF}}(k)}, \ldots, \frac{I_R(k+3)}{I_{R-\mathrm{PF}}(k-3)} ; \frac{I_S(k)}{I_{S-\mathrm{PF}}(k)}, \ldots, \frac{I_S(k+3)}{I_{S-\mathrm{PF}}(k-3)}; \frac{I_T(k)}{I_{T-\mathrm{PF}}(k)}, \ldots, \frac{I_T(k+3)}{I_{T-\mathrm{PF}}(k-3)}; I_0(k), \ldots, I_0(k+3) \right]. \quad (6)$$

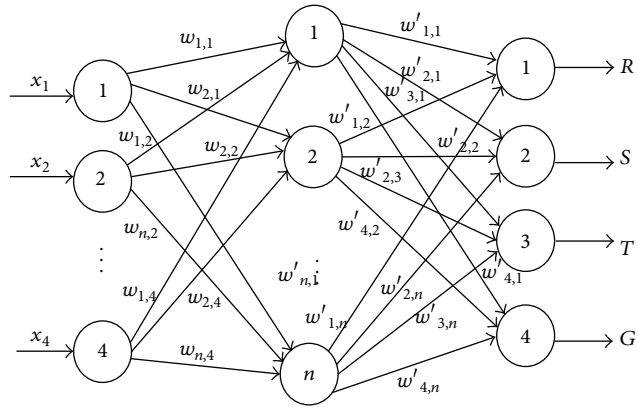

Figure 6: A feed-forward multilayer for the fault classifier (FC_1).

The ANN outputs related to FC_1 are called R, S, T, and G, which represent the three phases and the ground. If each of the outputs R, S, and T is near to 1 this indicates that fault occurred in this phase. When the output G takes the value 1, in this case the fault is related to ground. Taking the following example, if the fault classifier output is 0101, this indicates that the appearing fault is a single-phase fault which has occurred in the phase B and connected to ground (B-G). In the same context, an output 0110 shows that the fault which has occurred is a two-phase fault (B-C).

The second proposed fault classifier (FC_2) used the modular ANN approach. The proposed approach based on fault classification consists of four independent artificial neural networks, one for each phase (R, S, and T) and another for faults involving ground (G), which are called ANN-R, ANN-S, ANN-T, and ANN-G, respectively. The ANNs inputs are the samples of currents signals and the outputs are presented by the logic values (0 or 1). All network outputs are integrated to determine the fault type via a logic circuit; see Figure 7. Each network designed (ANN-i with $i = R, S,$ and T) treated four prefault and four postfault samples for each phase current. Thus the ANN-G treats four samples of zero sequence current. Figure 6 shows the schematic diagram of the proposed fault classification algorithm. Consequently, the input numbers selected for each ANN-j($j = \{R, S, T, G\}$) is equal to four currents samples. Thus, the total inputs number necessary to carry out the fault classification task via the modular ANN technique is equal to 16 normalized samples. The input vector of each ANN-i ($i = R, S,$ and T) is called $X^i_{\mathrm{FC}_2}$ and for ANN-G is called $X^G_{\mathrm{FC}_2}$ shown by the following equation system:

$$X^i_{\mathrm{FC}_2} = \left[\frac{I_i(k)}{I_{i-\mathrm{PF}}(k)}, \ldots, \frac{I_i(k+3)}{I_{i-\mathrm{PF}}(k-3)} \right] \quad i = \{R, S, T\}, \qquad X^G_{\mathrm{FC}_2} = \left[I_0(k), \ldots, I_0(k+3) \right]. \quad (7)$$

The suggested modular structure of the proposed fault classifier (FC_2) based on four independent artificial neural

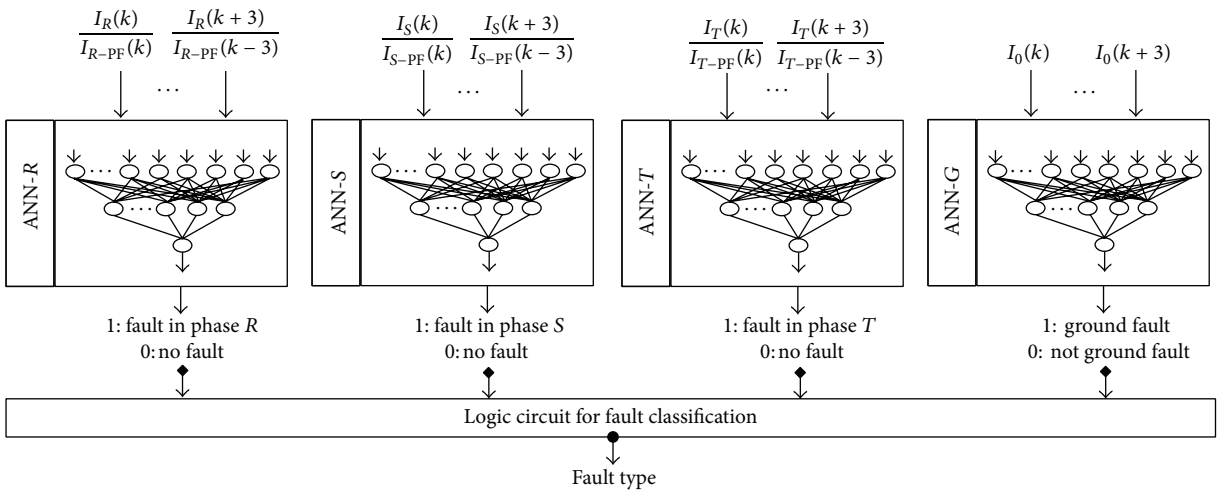

Figure 7: Modular ANN-based fault classifier (FC_2).

Table 1: Neural network desired outputs.

Type of faults	Desired network outputs			
	R	*S*	*T*	*G*
R-*G* fault	1	0	0	1
S-*G* fault	0	1	0	1
T-*G* fault	0	0	1	1
R-*S* fault	1	1	0	0
R-*T* fault	1	0	1	0
T-*S* fault	0	1	1	0
R-*S*-*G* fault	1	1	0	1
R-*T*-*G* fault	1	0	1	1
T-*S*-*G* fault	0	1	1	1
R-*S*-*T* fault	1	1	1	0

networks (ANN-*R*, ANN-*S*, ANN-*T*, and ANN-*G*) at four outputs is detailed in Figure 7. Each artificial neural network (ANN-*R*, ANN-*S*, and ANN-*T*) is designed to indicate the presence or not of a fault in related phases (*R*, *S*, and *T*), and the ANN-*G* is designed to indicate the involvement or not of the ground throughout the fault. Thus the ANNs outputs take the logic value (0 or 1), indicating the absence or the presence of a fault on the corresponding phase (*R*, *S*, and *T*) and if the fault is related to ground or not (*G*). We notice that the outputs admitting a value higher than 0.9 will be considered to be active (presence of fault) and the outputs having a value smaller than 0.1 (absence of fault) will be considered to be inactive. The various possible combinations can design the fault type. The proposed modular neural network should be able to distinguish with precision between the ten faults types affecting one transmission line. The neural network desired outputs for all the ten fault types are shown in Table 1.

4.1.2. Training Data. To lead to optimal and effective ANN architectures conceived for the fault classification task for the two suggested fault classifiers (FC_1 and FC_2), a suitable number of representative examples of the phenomenon in question must be selected. Moreover, the neural networks ANNs can learn the fundamental characteristics of the problem and provide correct outputs in new situations which are not considered during the training process. In order to train each ANN to obtain sufficient examples, we considered various fault scenarios at different fault conditions such as different fault locations (between 0 and 100% of line length) with various fault resistances R_f (0.1, 100 Ω) and various fault inception angles FIA (0 and 90°). The number of these full scenarios is 10 fault locations ∗ 2 fault resistances ∗ 2 fault inception angles ∗ 10 fault types = 400 fault cases destined for the ANN training process. The parameter values used to generate the data training sets and the ANN tests models for the two adopted fault classifier types are illustrated in Table 2.

Table 2: Training and test generation data of FC_1 and FC_2.

Parameter	Training	Testing
Fault type	*L*-*g*: *R*-*G*, *S*-*G*, *T*-*G* *L*-*L*: *R*-*S*, *R*-*T*, *T*-*S* *L*-*L*-*g*: *R*-*S*-*G*, *R*-*T*-*G*, *T*-*S*-*G*, *L*-*L*-*L*: *R*-*S*-*T*	*L*-*g*: *R*-*G*, *S*-*G*, *T*-*G* *L*-*L*: *R*-*S*, *R*-*T*, *T*-*S* *L*-*L*-*g*: *R*-*S*-*G*, *R*-*T*-*G*, *T*-*S*-*G*, *L*-*L*-*L*: *R*-*S*-*T*
Fault location L_f (km)	1, 10, 20, 30, . . . , 80, and 90 km	12, 56, 78, and 94
Fault inception angle FIA (°)	0° and 180°	0°, 75°, 135°, and 225°
Fault resistance R_f (Ω)	0.1 and 100 Ω	2, 33, 99, and 199

4.1.3. Structure of the Neural Fault Classifier. The determination of hidden layers number and the number of neurons per layer is very important considering that it affects the training time and the generalization property of the neural network. The most used approach to find adequate architectures is based mainly on the various tests and various network configurations. After a series of ANN structure tests and

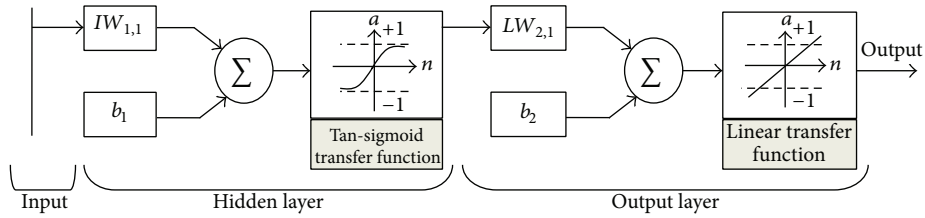

Figure 8: Architecture of ANN-based fault classifier (FC_1 and FC_2).

Table 3: Architecture of modular ANN-based fault classifier (FC_2).

Modular ANN-based fault classifier	Architecture	Mean square error (MSE)	Number of epochs
ANN-*R*	4-6-1	$5.91e-06$	12
ANN-*S*	4-5-1	$7.85e-06$	14
ANN-*T*	4-8-1	$4.88e-06$	10
ANN-*G*	4-6-1	$5.97e-06$	13

modification, the best architecture obtained of each ANN is that which provides satisfactory results. In this work, the best performance of the two proposed fault classifiers (FC_1 and FC_2) is obtained by the three-layer neural network. For all ANNs used for the two proposed fault classifiers (FC_1 and FC_2), a "tan-sigmoid" function was used as activation function of the input layer and "purelin" function in the output layer. Figure 8 shows the architecture of each ANN based on fault classifier (FC_1 and FC_2).

The numbers of hidden layer neuron for single ANN approach based fault classifier (FC_1) are chosen initially as 5 and then increased in step to 10, 15, 20, 25 to 30 as described above. The best performance is achieved by using a three-layer neural network with 16 inputs and 4 outputs, and the optimal number of neurons in the hidden layer was found to be 30 neurons. In this learning strategy, the mean square error (mse) decreases in 100 epochs to $6.67e{-}06$ in around 8 min and 35 sec learning time on a PC (P4, 2.13 GHz, 2 GB RAM). The single ANN approach based fault classifier (FC_1) requires large training sets and long training time. Also the network complexity is higher, and it has slower learning capability. Although the procedure for development of the architecture of modular ANN-based fault classifier is the same as that of single ANN-based fault classifier, the training time is very less for modular networks approximately 1 min and 49 sec for all four modules and the final architecture of modular ANN-based fault classifier is shown in Table 3.

4.1.4. Testing of the Fault Classifier. In order to evaluate the performances of the proposed fault classification algorithms (FC_1 and FC_2) based, respectively, on the single neural network approach and the modular artificial neural networks approach, we consider various fault scenarios more than those taken into account during the training process. These scenarios are subjected under various fault conditions such as different fault locations L_f, different fault resistances R_f, and different fault inception angles FIA. The tests results of the two proposed fault classifiers (FC_1 and FC_2) are presented in Table 4.

The simulation results prove well the precision of the two proposed algorithms. Indeed ANN outputs converge to the desired values (either very near to zero or one). However, it can be seen that, from the tests results presented in Table 4, the modular artificial neural network based on fault classifier (FC_2) is more precise than the single artificial neural network based on fault classifier (FC_1) since the first one converges towards the desired results with a minimum error compared to the second classifier.

An output of 0.8 or 0.9, given by one of the two suggested fault classification algorithms, represents the same result in fault classification task and indicates at the same time a faulty phase, whereas, for a fault location task, an output of 0.8 implies a fault produced at a distance of 80% from the line length and an output of 0.9 means that the fault is produced at a distance of 90% from the line length. The fault location requires more precision than the fault classification. So the use of single ANN approach for the fault location task presents disadvantages such as complexity, ANN long training time, and less accuracy compared to the modular ANN approach, as already seen for the fault classification task. Consequently, in order to estimate the exact fault location, it was decided to develop an accurate fault location algorithm based on modular artificial neural networks.

4.2. Fault Location. The proposed fault location algorithms in this part are based on the modular ANN approach. In this approach, during the appearance of a fault in transmission line, the fault detection and fault classification units identify the fault appearance and its type. Then it activates the fault location unit. The fault classification unit will be capable of determining the fault type if it is single line to ground (*L-G*), double lines (*L-L*), double lines to ground (*L-L-G*), or three-line fault (*L-L-L*). The proposed fault classification unit based on modular ANN approach detects and identifies the fault type. Thus the outputs generated by the fault classification unit activate the particular module of fault locator; see Figure 9. The proposed fault location algorithm consists of four independent ANNs when each

Table 4: Results of the fault type classifier using single and modular ANN (FC_1 and FC_2).

Fault type	Fault location (Km)	Fault inception angle (°)	Fault resistance (Ω)	Network	Desired output				Actual output			
					A	B	C	D	A	B	C	D
A-G	12	25	0	Single ANN	1	0	0	1	1.1112	0.1281	0.1187	0.9287
				Modular ANN					1.0013	−0.0071	0.0004	1.0005
	94	225	199	Single ANN					0.9051	0.1266	0.1108	1.1290
				Modular ANN					1.0071	−0.0003	0.0037	1.0085
C-G	12	25	0	Single ANN	0	0	1	1	−0.0784	0.1420	1.1128	1.2940
				Modular ANN					0.0021	−0.0041	1.0093	0.9941
	94	225	199	Single ANN					0.1328	−0.1007	1.2871	1.1008
				Modular ANN					−0.0074	−0.0032	1.0078	0.9814
A-B-G	12	25	0	Single ANN	1	1	0	1	1.1850	0.9072	0.0088	0.9653
				Modular ANN					1.0085	1.0066	−0.0042	1.1473
	94	225	199	Single ANN					1.0951	0.9552	0.1178	1.1008
				Modular ANN					1.0082	1.0077	−0.0004	0.9993
B-C-G	12	25	0	Single ANN	0	1	1	1	0.1136	1.0951	0.9867	1.1000
				Modular ANN					−0.0031	0.9972	1.0007	1.0081
	94	225	199	Single ANN					0.1807	1.1009	1.1150	1.087
				Modular ANN					−0.0001	1.0023	1.0744	1.0003
A-B-C	12	25	—	Single ANN	1	1	1	0	0.9962	1.1007	1.1105	−0.1042
				Modular ANN					1.0087	1.0025	0.9992	0.0035
	94	225	—	Single ANN					0.9198	0.9289	1.1008	−0.1008
				Modular ANN					1.0008	1.0036	1.0089	0.0429

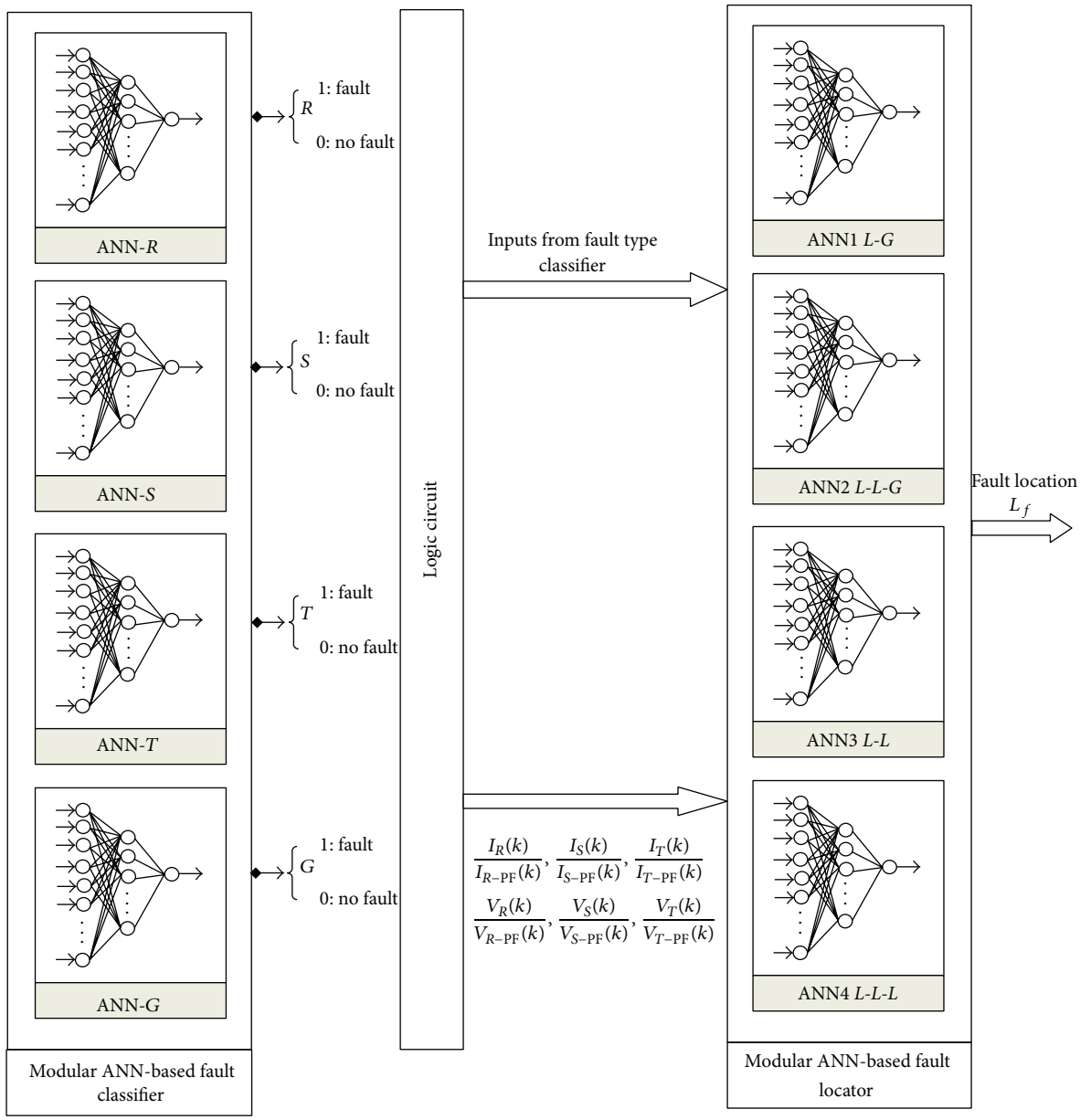

Figure 9: The proposed modular ANN-based fault locator.

fault type is trained by a neural network ANN-k with $k = \{L\text{-}G, L\text{-}L, L\text{-}L\text{-}G,$ and $L\text{-}L\text{-}L\}$. The block diagram of the proposed fault location is shown in Figure 9.

4.2.1. Inputs and Outputs. The determination of the inputs and outputs number presents the principal factor in determining the adequate size and the best architecture for the neural network. Hence, the sufficient inputs data to characterize the problem must be assured. In this context, three fault locators are presented. The first (FL_1) uses only the magnitudes of the fundamental components of three-phase currents, the second (FL_2) uses only the magnitudes of the fundamental components of three-phase voltages, and the third (FL_3) uses at the same time the magnitudes of the fundamental components of three-phase currents and voltages. The purpose of the fault location task is to estimate the exact fault location. Consequently, only obtained outputs by the fault location algorithm corresponding to the fault distance will be provided by the proposed modular neural network based on fault locator.

Thus we indicated by Input_{FL_1}, Input_{FL_2}, and Input_{FL_3} the inputs vectors taken by each proposed fault locator based on modular ANN approach:

$$\text{Input}_{FL_1} = \left[\frac{I_R(k)}{I_{R-PF}(k)}, \frac{I_S(k)}{I_{S-PF}(k)}, \frac{I_T(k)}{I_{T-PF}(k)}\right],$$

$$\text{Input}_{FL_2} = \left[\frac{V_R(k)}{V_{R-PF}(k)}, \frac{V_S(k)}{V_{S-PF}(k)}, \frac{V_T(k)}{V_{T-PF}(k)}\right],$$

Table 5: Training and test generation data of FL_1, FL_2, and FL_3.

Parameter	Training	Testing
Fault type	*L-g*: *R-G*, *S-G*, *T-G* *L-L*: *R-S*, *R-T*, *T-S* *L-L-g*: *R-S-G*, *R-T-G*, *T-S-G*, *L-L-L*: *R-S-T*	***L-g***: *R-G*, *S-G*, *T-G* ***L-L***: *R-S*, *R-T*, *T-S* ***L-L-g***: *R-S-G*, *R-T-G*, *T-S-G*, ***L-L-L***: *R-S-T*
Fault location L_f (km)	1, 10, 20, 30, . . . , 80, and 90 km	05, 06, 07, 09, 12, 13, 14, 23, . . . , 90, 94, 96 km
Fault inception angle FIA (°)	0°, 180°, and 270°	5°, 10°, 25°, 40°, . . . , 225°, 315°, 360°
Fault resistance R_f (Ω)	0.1, 50, 100, and 150 Ω	2.6, 10, 22, 26, . . . , 190, 195 Ω

$$\text{Input}_{\text{FL}_3} = \left[\frac{I_R(k)}{I_{R-\text{PF}}(k)}, \frac{I_S(k)}{I_{S-\text{PF}}(k)}, \frac{I_T(k)}{I_{T-\text{PF}}(k)}, \frac{V_R(k)}{V_{R-\text{PF}}(k)}, \frac{V_S(k)}{V_{S-\text{PF}}(k)}, \frac{V_T(k)}{V_{T-\text{PF}}(k)} \right]. \tag{8}$$

The output for fault location task is given by

$$\text{Output}_{\text{FL}} = \left[L_f \right]. \tag{9}$$

4.2.2. Training Data. A large number of training data for different ANNs based on fault location task were generated using MATLAB software, taking into account various fault scenarios subjected under different fault conditions such as different fault locations L_f (1%, 10%, 20%, 30%, . . . , 90% of line length), different fault inception angles FIA (0°, 180°, and 270°), and various fault resistances R_f (0.1 Ω, 50 Ω, 100 Ω, and 150 Ω). Thus, the simulated fault numbers for the ANNs training process are equal to 648 for the fault related to ground: 6 (fault types) ∗ 9 (fault location) ∗ 4 (fault resistance) ∗ 3 (fault inception angles). For faults which did not involve ground the number of fault simulation is equal to 108 simulation cases: 9 (fault locations) × 4 (fault types) × 3 (fault inception angles). Consequently, the full number of simulated faults is 756. Table 5 presents the parameter values used to generate the data training sets and test models for the three proposed fault locators.

4.2.3. Structure of the Neural Fault Locator. Once the inputs and outputs numbers of each proposed fault locator based on the modular ANN are determined, it is necessary to determine the number of hidden layers and the number of neurons in each hidden layer. The major problems in the ANN architecture design are to make sure that the numbers of hidden layers and the number of neurons in each hidden layers converges to the adequate results (exact fault location with a minimum error) with a fast response time. ANNs architectures, including the input network number, the hidden layers number, and the neurons number in each hidden layer are given due to an experimental study with various network configurations. Through a series of tests and modifications of ANNs architectures, the final architecture for the different ANNs leads to the best performance that is obtained using a neural network with three layers. The number of neurons in the input layer corresponds to the inputs variable number in ANNs. The number of neurons in the hidden layers was given after a series of tests, and for the output layer only one neuron corresponds to the fault distance.

All computation time for the three adopted fault locators (FL_1, FL_2, and FL_3) is carried on a PC (P4, 2.13 GHz, and 2 GB RAM). The training time for the first fault locator (FL_1) is approximately 11 min and 35 sec for all four modules. For the second fault locator (FL_2) the training time is about 12 min and 31 sec for all four modules. The third fault locator (FL_3) has a training time equal to 8 min and 17 sec for all four modules. Hence, it can be seen that the third fault locator (FL_3), which uses current and voltage phasor magnitudes, presents a fast training time compared to the other fault locator algorithms.

The final architectures of the proposed modular ANN-based fault locator for each algorithm are given by Table 6.

4.2.4. Testing of the Fault Locator. Once the ANNs training procedure is entirely carried out, the fault locators FL_1, FL_2, and FL_3 based on modular ANN approach are tested with various fault scenarios which are not presented during the training process. These lasts are tested under various fault conditions, such as different fault location (L_f = 0–100% of the line length), different values of the fault resistances (R_f = 0–200 Ω), and various fault inception angles (FIA = 0°–360°). Furthermore, the influences of the fault condition variation were tested.

The percentage error relating to fault location task is based on the following equation:

$$\text{Absolute Error} = \frac{|\text{Estimated Distance} - \text{Actual Distance}|}{\text{Length of line}} * 100. \tag{10}$$

(1) Influence of the Fault Type and the Fault Location. Table 7 presents the effect of the fault type on the proposed fault location algorithms (FL_1, FL_2, and FL_3). Indeed, the examined fault types are phase-ground faults (*L-G*), phase-phase-ground faults (*L-L-G*), phase-phase faults (*L-L*), and phase-phase-phase faults (*L-L-L*). According to the test results in Table 7, the percentage error, for the fault location algorithm FL_1 which uses only currents magnitudes of the fundamental components (50 Hz) of three phases (*R*, *S*, and *T*), lies between 0.1007% and 1.4599%. For the algorithm

Table 6: Architectures of ANN based fault locators (FL_1, FL_2, and FL_3).

Modular ANN-based fault locator	Proposed fault locator	Architecture	Mean square error (MSE)	Training time (min)
1 phase to ground	FL_1	3-14-1	$4.23e-04$	2.80
	FL_2	3-16-1	$5.38e-03$	3.32
	FL_3	6-32-1	$9.71e-06$	2.43
Phase to phase	FL_1	3-16-1	$3.27e-04$	2.19
	FL_2	3-18-1	$4.99e-04$	2.92
	FL_3	6-28-1	$8.66e-05$	2.88
2 phases to ground	FL_1	3-13-1	$3.88e-03$	3.14
	FL_2	3-18-1	$4.99e-04$	3.28
	FL_3	6-30-1	$6.82e-05$	2.12
3 phases	FL_1	3-8-1	$3.62e-04$	2.82
	FL_2	3-14-1	$3.74e-04$	2.79
	FL_3	6-18-1	$7.33e-05$	2.34

FL_2 which uses only voltages magnitudes of the fundamental components (50 Hz) of three phases (R, S, and T), the percentage error varies between 0.1086% and 1.2862%. For the third proposed algorithm FL_3 using the magnitudes of the fundamental components of three-phase currents and voltages, the percentage error is within 0.0175% and 0.3041%. Thus, it can be seen from the test results that the proposed fault locator algorithm (FL_3) is more accurate than FL_1 and FL_2. Thus, the percentages errors prove well the capacity of the proposed modular ANN-based fault locator FL_3 to determine the exact fault distance, compared to FL_1 and FL_2.

(2) Influence of the Fault Resistance. The effect of the fault resistance on the precisions of the proposed fault location algorithms (FL_1, FL_2, and FL_3) was tested on the power system study. The simulation results given by Table 8 show the effects of R_f on accuracy of the proposed algorithms. In addition, these algorithms were tested for various fault resistances R_f for a "phase-ground fault (R-G)" among a fault distance equal to 75 Km and for an inception angle FIA equal to 10°. During the test the percentage error estimated by the proposed fault location algorithms lies between 0.1111% and 1.2019% for FL_1, 0.2218% and 1.9713% for FL_2, and 0.0912% and 0.3071% for FL_3. Consequently, the proposed modular ANN-based fault locator uses the magnitudes of the fundamental components of three-phase currents and voltages (FL_3), is highly accurate compared to FL_1 and FL_2, and is practically independent of the fault resistance.

The criteria for evaluating the performance characteristics of the proposed fault locator based on modular ANN are translated by the stability of ANN output values in the normal situation and in the fault situation. Thus, minimal response time T_r, which presents the difference between the fault appearance time T_f and the time T_e where the ANN output indicates the exact fault location, is expressed as follows:

$$T_r = T_f - T_e. \tag{11}$$

The best ANN based on fault locator is obtained by the stability of ANN outputs under minimal response time. Therefore, the ANN output is stable in the normal situation and in the fault situation and capable of providing fast and exact fault location with a wide variety of fault conditions. In our study case the ANN-based fault locator is trained to show the output as 110 Km for no fault situation or for fault outside the line segment. For faults which appeared on the line segment, the ANN is trained to show the output as the exact fault position.

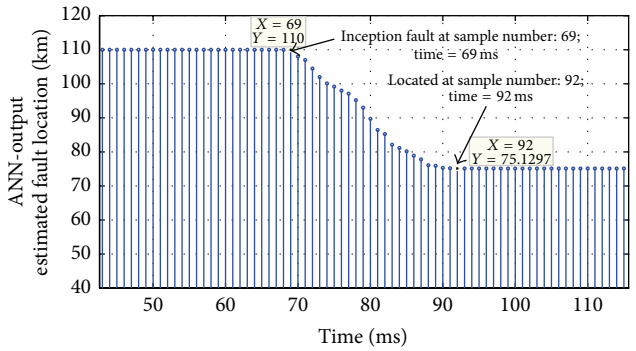

Figure 10: Test result of FL_3 during R-G fault with $L_f = 75$ Km, $R_f = 200\,\Omega$, and FIA = 10°.

In a perspective to evaluate the response time of the proposed algorithm, we simulated a single phase to ground fault (R-G) with $L_f = 75$ km, $R_f = 200\,\Omega$, and a fault inception angle FIA = 10° corresponding to the occurrence fault at time 69 ms; see Figure 10. The output of the proposed fault location algorithm FL_3 converges to 75.1297 km at time equal to 92 ms as against the set value of 75 km. The response time T_r of the proposed algorithm is about 23 ms. This proves that the modular ANN-based fault locator responds quickly to the desired outputs with minimum error.

(3) Influence of the Fault Inception Angle. In practice, the faults can occur at any line location; that is, the fault inception angle FIA cannot be defined in advance. Thus, it is important to check the performance of the proposed algorithm with various fault inception angles FIA. In this context, we simulated a double phase to ground fault with

Table 7: The effect of the fault type and the location of modular ANN-based fault locators (FL_1, FL_2, and FL_3).

Fault type	Fault location (Km)	Fault inception angle (°)	Fault resistance (Ω)	Output of ANN-based FL_1 (Km)	Output of ANN-based FL_2 (Km)	Output of ANN-based FL_3 (Km)	Percentage error of ANN-based FL_1 (%)	Percentage error of ANN-based FL_2 (%)	Percentage error of ANN-based FL_3 (%)
Single line to ground faults (*L-g*)	07	325	26	06.8971	07.1137	07.0196	0.1029	0.1137	0.0196
	13	125	130	13.4461	12.5841	12.7410	0.4461	0.4159	0.2590
	23	145	2.6	22.6988	23.3415	22.8875	0.3012	0.3415	0.1125
	34	275	195	35.2511	35.1286	34.2173	1.2511	1.1286	0.2173
	47	5	120	46.1081	47.4954	47.2511	0.8919	0.4954	0.2511
	58	25	95	57.0910	58.3599	58.1271	0.9090	0.3599	0.1271
	66	215	122	67.1241	66.9714	66.2791	1.1241	0.9714	0.2791
	75	10	53	75.6487	74.4259	74.8118	0.6487	0.5741	0.1882
	83	40	144	82.1475	81.9471	82.8334	0.8525	1.0529	0.1666
	96	135	125	94.5401	97.0778	95.7126	1.4599	1.0778	0.2874
Double line to ground faults (*L-L-g*)	09	25	10	10.1712	09.1783	9.0708	0.1712	0.1783	0.0708
	14	55	2.6	13.8277	13.8054	13.9271	0.1723	0.1946	0.0729
	26	125	190	24.9810	24.7138	25.7297	1.0190	1.2862	0.2703
	38	225	70	38.5714	38.4293	38.1866	0.5714	0.4293	0.1866
	44	315	95	44.9141	44.9785	44.2317	0.9141	0.9785	0.2317
	52	360	55	52.7129	52.6129	52.1711	0.7129	0.6129	0.1711
	63	120	170	62.1259	64.0709	62.7199	0.8741	1.0709	0.2801
	78	90	99	78.8012	77.0878	78.1531	0.8012	0.9122	0.1531
	88	120	65	88.1150	86.8019	87.8914	1.1150	1.1981	0.1086
	92	75	120	92.9908	93.1599	92.1705	0.9908	1.1599	0.1705
Line to line faults (*L-L*)	06	325	—	06.2371	05.8914	05.9825	0.2371	0.1086	0.0175
	16	125	—	16.1099	16.2514	16.0180	0.1099	0.2514	0.0180
	22	145	—	22.4147	21.9471	22.3041	0.4147	0.0529	0.3041
	31	275	—	31.1945	34.1286	30.9197	0.1945	0.1286	0.0803
	45	5	—	45.3274	45.2748	45.0923	0.3274	0.2748	0.0923
	54	25	—	54.2998	55.0074	54.1359	0.2998	1.0074	0.1359
	67	215	—	67.1929	67.2387	66.8147	0.1929	0.2387	0.1853
	77	10	—	77.4128	76.7035	76.8041	0.4128	0.2965	0.1959
	82	40	—	82.4511	82.6326	81.9033	0.4511	0.6326	0.0967
	90	135	—	90.7080	92.8615	90.2734	0.7080	0.8615	0.2734
Three -line faults (*L-L-L*)	05	25	—	05.1288	05.1431	04.9212	0.1288	0.1431	0.0788
	12	55	—	12.1007	12.2041	12.0704	0.1007	0.2041	0.0704
	23	125	—	23.2051	22.7733	23.1097	0.2051	0.2267	0.1097
	36	225	—	35.8134	35.2010	36.0914	0.1866	0.7990	0.0914
	42	315	—	42.1275	41.7187	42.0868	0.1275	0.2813	0.0868
	57	360	—	57.3488	57.4009	56.8003	0.3488	0.4009	0.1977
	66	120	—	66.2914	65.2799	66.1277	0.2914	0.7201	0.1277
	74	90	—	73.6811	75.0719	73.8384	0.3189	1.0719	0.1616
	83	120	—	82.4087	83.6729	82.7337	0.5913	0.6729	0.2663
	94	75	—	95.9971	94.9129	94.2053	0.9971	0.9129	0.2053

Table 8: The effect of the fault resistance of modular ANN-based fault locators (FL_1, FL_2, and FL_3).

Fault conditions			Desired output (Km)	Actual output (Km)			Error (%)		
Fault type	FIA (°)	R_f (Ω)		FL_1	FL_2	FL_3	FL_1	FL_2	FL_3
R-G	10°	0	75	74.8889	75.3175	75.0912	0.1111	0.3175	0.0912
R-G	10°	10	75	74.7792	74.7782	75.1008	0.2208	0.2218	0.1008
R-G	10°	100	75	75.8217	75.3390	73.7193	0.8217	1.3390	0.2807
R-G	10°	150	75	75.8944	75.6008	75.3071	0.8944	0.6008	0.3071
R-G	10°	200	75	76.2019	76.9713	75.1297	1.2019	1.9713	0.1297

Table 9: The effect of the fault inception angle of modular ANN-based fault locators (FL_1, FL_2, and FL_3).

Fault conditions			Desired output (Km)	Actual output (Km)			Error (%)		
Fault type	R_f (Ω)	FIA (°)		FL_1	FL_2	FL_3	FL_1	FL_2	FL_3
R-S-G	33	30°	11	11.3129	10.9023	11.0009	0.3129	0.0977	0.0009
R-S-G	33	60°	11	10.6189	10.7948	10.8984	0.3811	0.2052	0.0967
R-S-G	33	90°	11	11.2009	11.2078	11.1299	0.2009	0.2078	0.1299
R-S-G	33	180°	11	11.3914	11.5851	11.1007	0.3914	0.4149	0.1007
R-S-G	33	360°	11	11.4015	11.4197	10.8392	0.4015	0.4197	0.1608

Table 10: The effect of critical fault condition of modular ANN-based fault locators (FL_1, FL_2, and FL_3).

Fault conditions			Desired output (Km)	Actual output (Km)			Error (%)		
Fault type	FIA (°)	R_f (Ω)		FL_1	FL_2	FL_3	FL_1	FL_2	FL_3
S-G	360°	199	96	93.7422	93.5863	95.8197	2.2578	2.4137	0.1803
S-T	360°	—	96	96.7001	96.8100	95.7881	0.7001	0.8100	0.2119
S-T-G	360°	199	96	93.8066	97.9806	96.3011	2.1934	1.9806	0.3011
R-S-T	360°	—	96	95.0009	97.1732	96.2999	0.9991	1.1732	0.2999

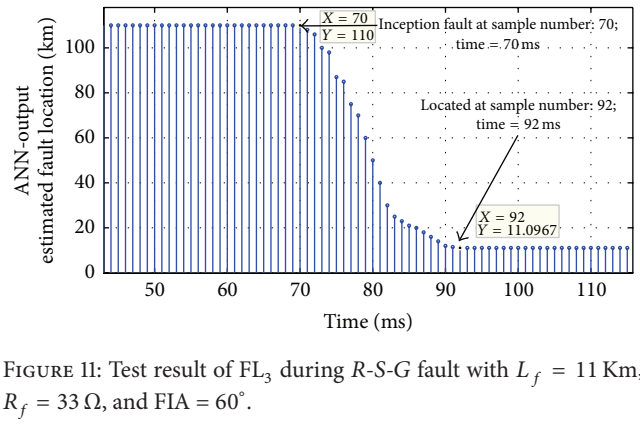

Figure 11: Test result of FL_3 during *R-S-G* fault with $L_f = 11$ Km, $R_f = 33\,\Omega$, and FIA = 60°.

fault resistance $R_f = 33\,\Omega$, fault location $L_f = 11$ Km, and various fault inception angles FIA (30°, 60°, 90°, 180°, and 360°). The simulation results are presented in Table 9. It can be seen from these results that the percentage error for the estimation of the fault using FL_3 is between 0.0009% and 0.1608%, that of FL_1 is between 0.2009% and 0.4015%, and that of FL_2 lies between 0.0977% and 0.4197%. Consequently, it is clearly obvious that algorithm FL_3 is more accurately compared to other algorithms (FL_1 and FL_2). Consequently, the proposed algorithm (FL_3) is practically independent of the fault inception angle.

In order to show the fast convergence of the proposed algorithm FL_3 under the influence of fault inception angle FIA, a double phase to ground fault (*R-S-G*) with fault location $L_f = 11$ km, fault resistance $R_f = 33\,\Omega$, and fault inception angle FIA = 60°, a fault occurrence at time 70 ms was simulated; see Figure 11. We noticed that the fault locator (FL_3) makes it possible to locate the fault with a good precision and a fast convergence time. The fault occurrence at time $T_f = 70$ ms was located at time $T_e = 92$ ms at a distance $L_f = 11.0967$, which implies a fast response time about $T_r = 22$ ms and a precision of 0.0967%. Thus it is clear that the proposed fault locator based on modular ANN (FL_3) can accurately locate the fault with high fault inception angle FIA.

(4) Influence of Critical Fault Conditions. In this context, we simulated various fault types under extreme fault conditions such as maximum fault resistance ($R_{f\max}$), maximum fault inception angle (FIA_{max}), and a fault location created at 96 Km for the transmission line ($L_{f\max}$). Hence, the three proposed algorithms were tested on the four fault types and the simulation results are illustrated in Table 10. Thus, it can be seen that the proposed algorithm FL_3 is more accurate and presents high performances especially for critical fault conditions compared to other algorithms FL_1 and FL_2. The corresponding percentage error represents very satisfactory results.

Table 11: Comparison of ANN-based fault classification and location schemes.

Algorithms suggested	Fault classifier inputs	Fault locator inputs	FIA range (°)	L_f range (%)	R_f range (Ω)	%Error range	Response time
Joorabian et al. [22]	Five consecutive samples of three-phase currents and voltages	Five consecutive samples of three-phase currents and voltages	0–90°	0–94%	0–100	0.0397% to 0.4123%	Not indicated
Mahanty and Gupta [10]	Five consecutive samples of three-phase currents	Five consecutive samples of three-phase currents and voltages	0–90°	0–82%	0–200	0.0007% to 4.45%	Not indicated
Jiang et al. [31]	Negative-sequence components of three-phase currents and voltages quantities	Negative-sequence components of three-phase currents and voltages quantities	Not indicated	Not indicated	Not indicated	0.41% to 0.54%	1.28 cycles
Yadav and Thoke [32]	No method for fault classification	Three consecutive samples of three-phase currents and voltages	Not indicated	0–90%	0–100	0.052% to 1.5693%	1.5 cycles
Proposed scheme	Four consecutive samples of three-phase currents	Magnitudes of fundamental components of three-phase currents and voltages	0–360°	0–96%	0–200	0.0175% to 0.3041%	1 cycle time from inception of fault

In the same way, this algorithm is qualified effective since it presents a fast response time in convergence to the desired results. Indeed, we simulated two phases to ground faults (S-T-G) at time 75 ms with $L_{f\max} = 96$ km, $R_{f\max} = 199\,\Omega$, and a fault inception angle FIA = 360°; see Figure 12. We noticed that the proposed fault locator (FL_3) located the fault at time $T_e = 100$ ms at a distance $L_f = 96.2999$ which implies a fast response time equal to $T_r = 25$ ms and a precision of 0.2999%; see Figure 12. This shows that the modular ANN-based fault locator converges correctly with fast time when the transmission line is affected by several faults under extreme fault conditions.

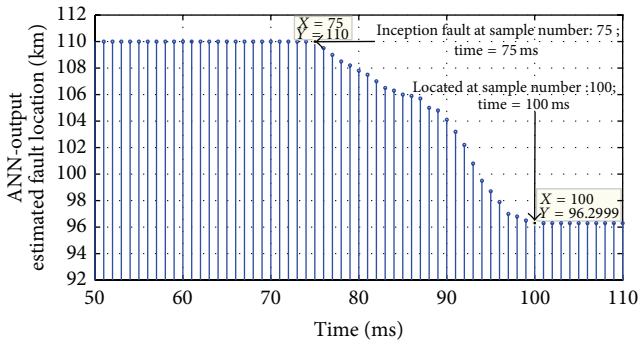

Figure 12: Test result of FL_3 during S-T-G fault with $L_f = 96$ Km, $R_f = 199\,\Omega$, and FIA = 360°.

5. Comparison between Proposed and Existing Schemes

The suggested fault classification and location algorithms, based on modular ANN, are compared with some former works. These proposed algorithms are developed for all the ten fault types, which can affect a transmission line, under various fault conditions such as wider range of fault resistance R_f, different fault inception angles FIA, and different fault location L_f. The main features of certain existing artificial neural network-based fault classification and location algorithms are presented in Table 11.

The accuracy of the proposed fault location algorithm (FL_3) lies between 0.0175% and 0.3041%, as indicated in Table 11. This shows the high performance of the (FL_3) algorithm and proves that it is more accurate than the existing algorithms. Thus in this present work, we proved that the response time of the proposed fault classification and fault location algorithms is estimated to one cycle from the fault occurrence. This response time is comparable to the classical distance relay protection [32].

6. Conclusion

An efficient fault classification and location algorithms in extra high voltage (EHV) transmission lines based on artificial neural networks were presented. For fault classification,

two algorithms were proposed: the first one used a single ANN approach, and the other used the modular ANN approach. Prefault and postfault samples of three-phase currents were used as inputs for these algorithms. A comparative study of the single and modular neural network shows that the modular approach gives more accuracy in order to identify the fault type. For fault location, three algorithms were developed. The first treats only the fundamental magnitudes of the three-phase currents samples, the second treats the fundamental magnitudes of the three-phase voltages samples, and the third uses the fundamental magnitudes of three-phase currents and voltages samples. The modular approach of neural networks was applied to evaluate these algorithms. The simulation results of these algorithms have been shown under a variety of fault situations such as different fault locations, different fault inception angles, and different fault resistances. The obtained results prove that the proposed modular ANN-based fault distance locator algorithm which uses fundamental magnitudes of three-phase currents and voltages is the most effective fault locator. The obtained results indicate that the proposed fault protection algorithm based on modular ANNs approach is capable of identifying all fault types and of estimating the exact fault location in the transmission lines with high accuracy. Moreover, the response of the proposed fault protection algorithm requires one cycle from the inception fault. Therefore, the modular ANN-based fault protection can be used for online fault classification and location in transmission lines.

Conflict of Interests

The authors declare that there is no conflict of interests regarding the publication of this paper.

References

[1] K. V. Babu, M. Tripathy, and A. K. Singh, "Recent techniques used in transmission line protection: a review," *International Journal of Engineering, Science and Technology*, vol. 3, no. 3, pp. 1–8, 2011.

[2] X. Dong, W. Kong, and T. Cui, "Fault classification and faulted-phase selection based on the initial current traveling wave," *IEEE Transactions on Power Delivery*, vol. 24, no. 2, pp. 552–559, 2009.

[3] E. Vázquez-Martínez, "A travelling wave distance protection using principal component analysis," *International Journal of Electrical Power and Energy System*, vol. 25, no. 6, pp. 471–479, 2003.

[4] D. Spoor and J. G. Zhu, "Improved single-ended traveling-wave fault- location algorithm based on experience with conventional substation transducers," *IEEE Transactions on Power Delivery*, vol. 21, no. 3, pp. 1714–1720, 2006.

[5] Y. Lin, C. Liu, and C. Chen, "A new PMU-based fault detection/location technique for transmission lines with consideration of arcing fault discrimination—part I: theory and algorithms," *IEEE Transactions on Power Delivery*, vol. 19, no. 4, pp. 1587–1593, 2004.

[6] W. Xiu and Y. Liao, "Accurate transmission line fault location considering shunt capacitances without utilizing line parameters," *Electric Power Components and Systems*, vol. 39, no. 16, pp. 1783–1794, 2011.

[7] C.-S. Chen, C.-W. Liu, and J.-A. Jiang, "A new adaptive PMU based protection scheme for transposed/untransposed parallel transmission lines," *IEEE Transactions on Power Delivery*, vol. 17, no. 2, pp. 395–404, 2002.

[8] J. Suonan, G. Song, Q. Xu, and Q. Chao, "Time-domain fault location algorithm for parallel transmission lines using unsynchronized currents," *International Journal of Electrical Power and Energy Systems*, vol. 28, no. 4, pp. 253–260, 2006.

[9] A. Ferrero, S. Sangiovanni, and E. Zappitelli, "Fuzzy-set approach to fault-type identification in digital relaying," *IEEE Transactions on Power Delivery*, vol. 10, no. 1, pp. 169–175, 1995.

[10] R. N. Mahanty and P. B. D. Gupta, "A fuzzy logic based fault classification approach using current samples only," *Electric Power Systems Research*, vol. 77, no. 5-6, pp. 501–507, 2007.

[11] O. A. S. Youssef, "A novel fuzzy-logic-based phase selection technique for power system relaying," *Electric Power Systems Research*, vol. 68, no. 3, pp. 175–184, 2004.

[12] P. K. Dash, A. K. Pradhan, and G. Panda, "A novel fuzzy neural network based distance relaying scheme," *IEEE Transactions on Power Delivery*, vol. 15, no. 3, pp. 902–907, 2000.

[13] B. Das and J. V. Reddy, "Fuzzy-logic-based fault classification scheme for digital distance protection," *IEEE Transactions on Power Delivery*, vol. 20, no. 2 I, pp. 609–616, 2005.

[14] J. S. R. Jang, "ANFIS: adaptive-network-based fuzzy inference system," *IEEE Transactions on Systems, Man and Cybernetics*, vol. 23, no. 3, pp. 665–685, 1993.

[15] S. Vasilic and M. Kezunovic, "Fuzzy ART neural network algorithm for classifying the power system faults," *IEEE Transactions on Power Delivery*, vol. 20, no. 2, pp. 1306–1314, 2005.

[16] N. Zhang and M. Kezunovic, "Coordinating fuzzy ART neural networks to improve transmission line fault detection and classification," in *Proceedings of the IEEE Power Engineering Society General Meeting (PES '05)*, pp. 734–740, San Francisco, Calif, USA, June 2005.

[17] J. Sadeh and H. Afradi, "Fault location scheme for combined transmission lines using artificial neural networks," in *Proceedings of the 22nd International Power System Conference (PSC '07)*, Tehran, Iran, November 2007, (Persian).

[18] S. M. Yeo, C. H. Kim, K. S. Hong et al., "A novel algorithm for fault classification in transmission lines using a combined adaptive network and fuzzy inference system," *International Journal of Electrical Power and Energy System*, vol. 25, no. 9, pp. 747–758, 2003.

[19] J. Sadeh and H. Afradi, "A new and accurate fault location algorithm for combined transmission lines using Adaptive Network-Based Fuzzy Inference System," *Electric Power Systems Research*, vol. 79, no. 11, pp. 1538–1545, 2009.

[20] P. K. Dash, A. K. Pradhan, and G. Panda, "Application of minimal radial basis function neural network to distance protection," *IEEE Transactions on Power Delivery*, vol. 16, no. 1, pp. 68–74, 2001.

[21] W. Lin, C. Yang, J. Lin, and M. Tsay, "A fault classification method by RBF neural network with OLS learning procedure," *IEEE Transactions on Power Delivery*, vol. 16, no. 4, pp. 473–477, 2001.

[22] M. Joorabian, S. M. A. T. Asl, and R. K. Aggarwal, "Accurate fault locator for EHV transmission lines based on radial basis function neural networks," *Electric Power Systems Research*, vol. 71, no. 3, pp. 195–202, 2004.

[23] Z. Chen and J. Maun, "Artificial neural network approach to single-ended fault locator for transmission lines," *IEEE Transactions on Power Systems*, vol. 15, no. 1, pp. 370–375, 2000.

[24] M. Al-Shaher, A. S. Saleh, and M. M. Sabry, "Estimation of fault location and fault resistance for single line-to-ground faults in multi-ring distribution network using artificial neural network," *Electric Power Components and Systems*, vol. 37, no. 7, pp. 697–713, 2009.

[25] J. Gracia, A. J. Mazón, and I. Zamora, "Best ANN structures for fault location in single- and double-circuit transmission lines," *IEEE Transactions on Power Delivery*, vol. 20, no. 4, pp. 2389–2395, 2005.

[26] G. Chawla, M. S. Sachdev, and G. Ramakrishna, "Artificial neural network applications for power system protection," in *Proceedings of the Canadian Conference on Electrical and Computer Engineering*, pp. 1954–1957, Saskatoon, Canada, May 2005.

[27] K. Z. Hassan and L. Zuyi, "An ANN based approach to improve the distance relaying algorithm," *Turkish Journal of Electrical Engineering and Computer Sciences*, vol. 14, no. 2, pp. 345–354, 2006.

[28] G. Banu and S. Suja, "ANN based fault location technique using one end data for UHV lines," *European Journal of Scientific Research*, vol. 77, no. 4, pp. 549–559, 2012.

[29] Y. Aslan, "An alternative approach to fault location on power distribution feeders with embedded remote-end power generation using artificial neural networks," *Electrical Engineering*, vol. 94, no. 3, pp. 125–134, 2012.

[30] A. Dasgupta, S. Nath, and A. Das, "Transmission line fault classification and location using wavelet entropy and neural network," *Electric Power Components and Systems*, vol. 40, no. 15, pp. 1676–1689, 2012.

[31] J. Jiang, C. Chuang, Y. Wang et al., "A hybrid framework for fault detection, classification, and location—part I: concept, structure, and methodology," *IEEE Transactions on Power Delivery*, vol. 26, no. 3, pp. 1988–1998, 2011.

[32] A. Yadav and A. S. Thoke, "Transmission line fault distance and direction estimation using artificial neural network," *International Journal of Engineering, Science and Technology*, vol. 3, no. 8, pp. 110–121, 2011.

[33] M. B. Hessine, H. Jouini, and S. Chebbi, "Fault detection and classification approaches in transmission lines using artificial neural networks," in *Proceedings of the IEEE Mediterranean Electrotechnical Conference (MELECON '14)*, pp. 520–524, Beirut, Lebanon, April 2014.

[34] M. B. Hessine, H. Jouini, and S. Chebbi, "A new and accurate fault classification algorithm for transmission lines using fuzzy logic system," *Wulfenia Journal*, vol. 20, no. 3, pp. 336–349, 2013.

[35] M. B. Hessine, H. Jouini, S. Chebbi, and S. Marrouchi, "Voltage and frequency stabilization of electrical networks by using load shedding strategy based on fuzzy logic controllers," *International Review of Electrical Engineering*, vol. 7, no. 5, pp. 5694–5704, 2012.

[36] R. Abbassi and S. Chebbi, "Energy management strategy for a grid-connected wind-solar hybrid system with battery storage: policy for optimizing conventional energy generation," *International Review of Electrical Engineering*, vol. 7, no. 2, pp. 3979–3990, 2012.

[37] K. Jemai, H. Jouini, and S. Chebbi, "Voltage stability control of electrical network using intelligent load shedding strategy based on fuzzy logic," *Mathematical Problems in Engineering*, vol. 2010, Article ID 341257, 17 pages, 2010.

[38] T. Bouthiba, "Fault location in EHV transmission lines using artificial neural networks," *International Journal of Applied Mathematics and Computer Science*, vol. 14, no. 1, pp. 69–78, 2004.

[39] E. A. Mohamed and N. D. Rao, "Artificial neural network based fault diagnostic system for electric power distribution feeders," *Electric Power Systems Research*, vol. 35, no. 1, pp. 1–10, 1995.

[40] A. I. Megahed and O. P. Malik, "An artificial neural network based digital differential protection scheme for synchronous generator stator winding protection," *IEEE Transactions on Power Delivery*, vol. 14, no. 1, pp. 86–93, 1999.

[41] M. R. Zaman and M. A. Rahman, "Experimental testing of the artificial neural network based protection of power transformers," *IEEE Transactions on Power Delivery*, vol. 13, no. 2, pp. 510–515, 1998.

[42] W. Wang, L. Li, H. Peng, J. Xiao, and Y. Yang, "Synchronization control of memristor-based recurrent neural networks with perturbations," *Neural Networks*, vol. 53, pp. 8–14, 2014.

[43] Y. Tang and W. K. Wong, "Distributed synchronization of coupled neural networks via randomly occurring control," *IEEE Transactions on Neural Networks and Learning Systems*, vol. 24, no. 3, pp. 435–447, 2013.

[44] W. Zhang, Y. Tang, J. Fang, and X. Wu, "Stability of delayed neural networks with time-varying impulses," *Neural Networks*, vol. 36, pp. 59–63, 2012.

[45] W. Zhang, Y. Tang, Q. Miao, and W. Du, "Exponential synchronization of coupled switched neural networks with mode-dependent impulsive effects," *IEEE Transactions on Neural Networks and Learning Systems*, vol. 24, no. 8, pp. 1316–1326, 2013.

[46] K. Hu, A. Song, M. Xia, X. Ye, and Y. Dou, "An adaptive filtering algorithm based on genetic algorithm-backpropagation network," *Mathematical Problems in Engineering*, vol. 2013, Article ID 573941, 8 pages, 2013.

[47] W. Chang, "An RBF neural network combined with OLS algorithm and genetic algorithm for short-term wind power forecasting," *Journal of Applied Mathematics*, vol. 2013, Article ID 971389, 9 pages, 2013.

[48] Y. Chang, J. Lin, J. Shieh, and M. F. Abbod, "Optimization the initial weights of artificial neural networks via genetic algorithm applied to hip bone fracture prediction," *Advances in Fuzzy Systems*, vol. 2012, Article ID 951247, 9 pages, 2012.

[49] E. Cuevas, D. Zaldívar, and P. Cisneros, "A swarm optimization algorithm for multimodal functions and its application in multicircle detection," *Mathematical Problems in Engineering*, vol. 2013, Article ID 948303, 22 pages, 2013.

[50] Y.-K. Lin, "Particle swarm optimization algorithm for unrelated parallel machine scheduling with release dates," *Mathematical Problems in Engineering*, vol. 2013, Article ID 409486, 9 pages, 2013.

[51] A. Liu and M. Yang, "A new hybrid nelder-mead particle swarm optimization for coordination optimization of directional overcurrent relays," *Mathematical Problems in Engineering*, vol. 2012, Article ID 456047, 18 pages, 2012.

[52] L. Li, Y. Yang, H. Peng, and X. Wang, "Parameters identification of chaotic systems via chaotic ant swarm," *Chaos, Solitons & Fractals*, vol. 28, no. 5, pp. 1204–1211, 2006.

[53] H. Peng, L. Li, Y. Yang, and F. Liu, "Parameter estimation of dynamical systems via a chaotic ant swarm," *Physical Review E*, vol. 81, no. 1, Article ID 016207, 2010.

[54] L. Li, Y. Yang, H. Peng, and X. Wang, "An optimization method inspired by "chaotic" ant behavior," *International Journal of Bifurcation and Chaos in Applied Sciences and Engineering*, vol. 16, no. 8, pp. 2351–2364, 2006.

[55] H. Peng, L. Li, J. Kurths, S. Li, and Y. Yang, "Topology identification of complex network via chaotic ant swarm algorithm," *Mathematical Problems in Engineering*, vol. 2013, Article ID 401983, 5 pages, 2013.

[56] K. N. Yu, H. T. Yau, and J.Y. Li, "Chaotic extension neural network-based fault diagnosis method for solar photovoltaic systems," *Mathematical Problems in Engineering*, vol. 2014, Article ID 280520, 9 pages, 2014.

[57] S. Abid, F. Fnaiech, and M. Najim, "A fast feed-forward training algorithm A modified form of the standard back-propagation algorithm," *IEEE Transactions on Neural Network*, vol. 12, no. 2, pp. 424–430, 2001.

[58] S. Abid, F. Fnaiech, B. W. Jervis, and M. Cheriet, "Fast training of multilayer perceptrons with a mixed norm algorithm," in *Proceedings of the IEEE International Joint Conference on Neural Networks (IJCNN '05)*, vol. 2, pp. 1018–1022, August 2005.

[59] S. Haykin, *Neural Networks: A Comprehensive Foundation*, Prentice Hall, Englewood Cliffs, NJ, USA, 1994.